# Investigations of Bivalent Antibody Binding on Fluid-Supported Phospholipid Membranes: The Effect of Hapten Density

Tinglu Yang, Olga K. Baryshnikova, Hanbin Mao, Matthew A. Holden, and Paul S. Cremer*

*Contribution from the Department of Chemistry, Texas A&M University, P.O. Box 30012, College Station, Texas 77843-3012*

Received November 25, 2002; E-mail: cremer@mail.chem.tamu.edu

***Abstract:*** Investigations of ligand−receptor binding between bivalent antibodies and membrane-bound ligands are presented. The purpose of these studies was to explore binding as a function of hapten density in a two-dimensionally fluid environment. A novel microfluidic strategy in conjunction with total internal reflection fluorescence microscopy was designed to achieve this. The method allowed binding curves to be acquired with excellent signal-to-noise ratios while using only minute quantities of protein solution. The specific system investigated was the interaction between anti-DNP antibodies and phospholipid membranes containing DNP-conjugated lipids. Binding curves for ligand densities ranging from 0.1 to 5.0 mol % were obtained. Two individual dissociation constants could be extracted from the data corresponding to the two sequential binding events. The first dissociation constant, $K_{D1}$, was $2.46 \times 10^{-5}$ M, while the second was $K_{D2} = 1.37 \times 10^{-8}$ mol/m$^2$. This corresponded to a positively cooperative binding effect with an entropic difference between the two events of $62.3 \pm 2.7$ J/(mol·K). Furthermore, the percentage of monovalently and bivalently bound protein was determined at each ligand density.

## Introduction

Ligand−receptor interactions are involved in a variety of biological processes such as cell signaling, pathogen identification, trafficking of lymphocytes, and the inflammatory response.[1,2] These binding events are often multivalent, and their properties can differ markedly from their monovalent constituents. Indeed, multivalent interactions may achieve higher binding affinity, afford larger contact areas between surfaces, allow signaling through oligomerization, and induce changes in the distribution of molecules at the membrane interface.[3] Examination of the binding modes and the thermodynamic characteristics of multivalency should provide critical insight into the nature of multivalent interactions and suggest strategies that might be employed for inhibiting them.[4] An understanding of the latter may prove crucial for discovering a broad range of pharmaceuticals with various functions such as the inhibition of viral entry or the termination of cancer metastasis.

We have recently demonstrated that microfluidic devices can be applied to the study of multivalent ligand−receptor interactions.[5] Such platforms offer many advantages over traditional analytical tools including high-throughput capabilities and vastly decreased reagent volumes. In fact, only 2 μL of protein solution is needed to collect each data point on a binding curve, and all the points can be obtained simultaneously. Another important feature is that microfluidic devices made of glass or poly-(dimethylsiloxane) (PDMS) can serve as supports for phospholipid bilayers, thus offering an attractive platform for studying multivalent ligand−receptor interactions on model biomembrane surfaces.[5] Supported lipid bilayers are two-dimensionally fluid, which enables them to mimic cell surface rearrangements.[6,7] A thin layer of water (∼10 Å thick)[8,9] between the bilayer and an underlying support serves as a lubricant and allows ligands bound to lipid molecules to undergo lateral rearrangements during the formation of multivalent contacts (Figure 1). Fluidity is expected to play a key role in binding enhancement on the surface of biological membranes, since a ligand for the second and subsequent binding events can be delivered through the lateral rearrangements of bilayer constituents. In supported lipid bilayers the concentration of lipids and associated ligands can be precisely controlled during preparation. Therefore, multivalent interactions on fluid surfaces can be explored over a wide range of ligand densities and other membrane chemistries incorporated into the two-dimensionally fluid bilayer.

* To whom correspondence should be addressed. Phone: (979) 862-1200. Fax: (979) 845-7561.

(1) Mammen, M.; Choi, S. K.; Whitesides, G. M. *Angew. Chem., Int. Ed.* **1998**, *37*, 2754−2794.
(2) Kiessling, L. L.; Pohl, N. L. *Chem. Biol.* **1996**, *3*, 71−77.
(3) Heldin, C. *Cell* **1995**, *80*, 213−223.
(4) Lees, W. J., Spaltenshtein, A., Kingery-Wood, L. E., Whitesides, G. M. *J. Med. Chem.* **1994**, *37*, 3419.
(5) Yang, T.; Jung, S. Y.; Mao, H.; Cremer, P. S. *Anal. Chem.* **2001**, *73*, 165−169.
(6) Hlavacek, W. S.; Posner, R. G.; Perelson, A. S. *Biophys. J.* **1999**, *76*, 3031−3043.
(7) Sackmann, E. *FEBS Lett.* **1994**, *346*, 3−16.
(8) Johnson, S. J.; Bayerl, T. M.; McDermott, D. C.; Adam, G. W.; Rennie, A. R.; Thomas, R. K.; Sackmann, E. *Biophys. J.* **1991**, *59*, 289−294.
(9) Cremer, P. S.; Boxer, S. G. *J. Phys. Chem. B* **1999**, *103*, 2554−2559.
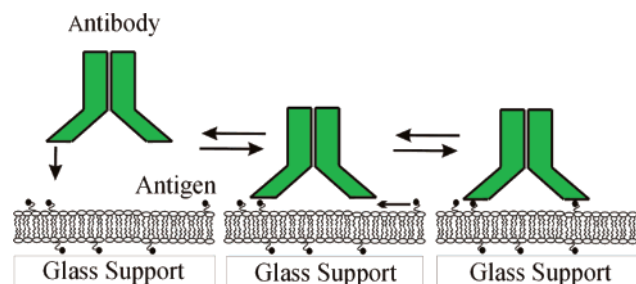
**Figure 1.** A schematic depiction of the role of membrane fluidity in bivalent interactions. Lateral movement of ligands and/or protein molecules is required to enable the second binding event. The diagram is not drawn to scale. Furthermore, no information about the orientation of the ligand with respect to the membrane surface should be inferred. In fact, some of the ligands may well be buried in the headgroup region of the membrane.

One of the most intensely studied multivalent binding systems involves the bivalent interaction between an antibody and two hapten moieties.[5,10–19] Very few studies, however, have looked at the relationship between hapten density and apparent binding constant. This is presumably because of the tedious, time-consuming nature and great expense of experiments performed without the benefit of a high-throughput, low-sample-volume assay. In fact, to the best of our knowledge, previous binding experiments on fluid membranes have been done with no more than three different ligand densities.[17] This is unfortunate because the most recent calculations for multivalent ligand–receptor binding now allow the effects of large proteins binding with small molecules at the membrane interface to be taken into account.[6] This would make it possible to devise simple models for determining both the first and second binding constants for antibody–antigen interactions at the biomembrane surface provided that binding curves are available for a sufficient number of antigen concentrations.

We performed a series of binding experiments inside microfluidic devices coated with supported lipid bilayers containing lipid-conjugated 2,4-dinitrophenyl moieties for binding with their associated IgG antibodies. Hapten density in the membranes was varied from 0.1 to 5.0 mol %. The results showed that the apparent dissociation constant, $K_{Dapp}$, tightened by about a factor of 10 over this range as the ligand density was increased. The majority of the changes took place between 0.1 and 3.75 mol %. A plot of available ligand density vs apparent dissociation constant afforded the determination of the individual binding constants for both the first and second binding events. It was found that the second binding event was less entropically costly than the first by $62.3 \pm 2.7$ J/(mol·K). This result is opposite of hapten binding to antibodies in bulk solution, where the second binding event is more entropically costly than the first.

An estimation of the fraction of protein which is monovalently and bivalently bound at each ligand density was also obtained.

## Experimental Section

**Fabrication of Microfluidic Devices**. Methods for fabrication of microfluidic devices were pioneered by Harrison, Manz, and Ramsey.[20,21] Subsequently, Biebuyck and co-workers showed that microchannels could be formed between poly(dimethylsiloxane) molds and glass surfaces for use with biological materials.[22] In our laboratory, designs for microfluidic channels were created using Corel Draw software. The fabrication procedure included printing images with a 1200 dpi printer followed by photographic reduction of the printed patterns, which transferred the images onto black and white high-contrast Kodak technical pan film. The film was used as a photomask for 1:1 photolithography. Glass slides were spin coated with photoresist and exposed to UV light through the photomasks. After treatment with developing solution, regions protected with the photomask created a patterned master plate around which PDMS was cured to form an elastomeric mold. The mold was carefully peeled off, and inlets and outlets could be added by puncturing the elastomer with a hollow needle. The stamp was repeatedly washed with acetone and deionized water in an alternating fashion. The final device was formed by placing the lithographically patterned PDMS mold into contact with a planar borosilicate coverslip after brief treatment of both in an oxygen plasma. Exposure to the oxygen plasma was important for rendering the PDMS surface hydrophilic.[23,24]

**Solid Supported Lipid Bilayers**. Once hydrophilic microchannels were formed, small unilamellar vesicles (SUVs) in phosphate buffer solution (PBS) were immediately injected through the inlets. The SUVs were prepared by standard methods described elsewhere.[5,25,26] Briefly, lipids were dissolved in chloroform and allowed to dry under a stream of nitrogen followed by desiccation under vacuum for 2 h. The lipids were reconstituted in PBS buffer (pH 7.2) and extruded more than seven times through polycarbonate filters with 50 nm pores. Upon injection into a microfluidic device, the lipid vesicles spontaneously fused to the glass and PDMS surfaces to form a continuous lipid bilayer coating.[5,27] Excess vesicles could then be flushed away with pure buffer. The quality of the supported bilayers on the glass surface was verified by fluorescence recovery after photobleaching (FRAP) as this surface was used to take data for all subsequent experimental measurements. Supported bilayers in this study consisted of egg phosphatidylcholine (egg PC; Avanti Polar Lipids, Alabaster, AL), fluorescein–phosphoethanolamine (Molecular Probes, Eugene, OR), and *N*-dinitrophenyl-aminocaproyl phosphatidylethanolamine (DNP-cap PE; Avanti Polar Lipids, Alabaster, AL), which served as the hapten moiety. It was assumed in all studies presented herein that the concentrations of hapten in the upper and lower leaflets of the bilayer were similar.

**Preparation of Antibodies**. Polyclonal anti-dinitrophenyl-KLH IgG antibodies were purchased from Molecular Probes and labeled with Alexa 594 dye using a standard antibody-labeling kit (A10239, Molecular Probes, Eugene, OR). Labeling yielded ~1.6 fluorophores/protein as determined by UV absorption spectroscopy. It is known that the maximum surface coverage of an IgG on a supported membrane is close to 6000 molecules/$\mu m^2$.[16] Since the self-quenching of this dye is

(10) Stanton, S. G.; Kantor, A. B.; Petrossian, A.; Owicki, J. C. *Biochim. Biophys. Acta* **1984**, *776*, 228–236.
(11) Mammen, M.; Gomez, F. A.; Whitesides, G. M. *Anal. Chem.* **1995**, *67*, 3526–3535.
(12) Nieba, L., Krebber, A., Pluckthun, A. *Anal. Biochem.* **1996**, *234*, 155–165.
(13) Sapsford, K. E., Liron, Zvi., Shubin, Y. S., Ligler, F. S. *Anal. Biochem.* **2001**, *73*, 5518–5524.
(14) Thompson, N. L.; Drake, A. W.; Chen, L.; Broek, W. V. *Photochem. Photobiol.* **1997**, *65*, 39–46.
(15) Thompson, N. L.; Poglitsch, C. L.; Timbs, M. M.; Pisarchick, M. L. *Acc. Chem. Res.* **1993**, *26*, 567–573.
(16) Pisarchick, M. L.; Thompson, N. L. *Biophys. J.* **1990**, *58*, 1235–1249.
(17) Kalb, E., Engel, J., Tamm, L. K. *Biochemistry* **1990**, *29*, 1607–1613.
(18) Uzgiris, E. E., Kornberg, R. D. *Nature* **1983**, *301*, 125.
(19) Nygren, H., Werthen, M., Stenberg, M. *J. Immunol. Methods* **1987**, *101*, 63–71.

(20) Harrison, D. J.; Fluri, K.; Seiler, K.; Fan, Z. H.; Effenhauser, C. S.; Manz, A. *Science* **1993**, *261*, 895–897.
(21) Jacobson, S. C.; Hergenroder, R.; Koutny, L. B.; Ramsey, J. M. *Anal. Chem.* **1994**, *66*, 2369–2373.
(22) Delamarche, E.; Schmid, H.; Michel, B.; Biebuyck, H. *Adv. Mater.* **1997**, *9*, 741–746.
(23) Deng, T.; Wu, H.; Brittain, S. T.; Whitesides, G. M. *Anal. Chem.* **2000**, *72*, 3176–3180.
(24) Duffy, D. C.; McDonald, J. C.; Schueller, O. J. A.; Whitesides, G. M. *Anal. Chem.* **1998**, *70*, 4974–4984.
(25) Nollert, P.; Kiefer, H.; Jahnig, F. *Biophys. J.* **1995**, *69*, 1447–1455.
(26) Kalb, E.; Frey, S.; Tamm, L. K. *Biochim. Biophys. Acta* **1992**, *1103*, 307–316.
(27) Mao, H., Yang, T., Cremer, P. S. *Anal. Chem.* **2002**, *74*, 379–385.

relatively low,[28] the fluorescence yield obtained in the experiments presented here is expected to be linearly proportional to the protein concentration at the interface in agreement with previous work.[16,29,30] The dye-labeled protein was concentrated to 27.8 $\mu$M by using centrifugal filter devices (Centricon, Millipore) without changing its pH or ionic strength. The material was stored in a pH 7.2 buffer solution containing 0.01 M sodium phosphate, 0.15 M NaCl, and 0.2 mM sodium azide.

**Epifluorescence Microscopy and Total Internal Reflection Fluorescence Microscopy**. Fluorescent images of the supported membranes and antibodies in the microchannels were obtained by epifluorescence microscopy (E800 fluorescence microscope, Nikon) using a 10× objective. Total internal reflection fluorescence microscopy (TIRFM) was performed to discriminate between antibodies in solution and those bound to the surface.[31] This experiment was conducted by reflecting a 1 mW 594 nm helium neon laser beam (Uniphase, Manteca, CA) off the sample surface through a dove prism optically coupled to the planar coverslip surface through immersion oil. The laser beam was telescoped out with a 5× lens set to create an intensity profile that varied less than 3% across the width of the microchannel array. The evanescent wave generated at the interface decayed exponentially to its 1/$e$ value by 70 nm from the surface under the conditions employed.[5,32,33] This allowed information about proteins bound to the supported lipid bilayer to be obtained with high specificity. All images were captured on a Photometrics Sensys CCD camera, stored using Metamorph software from Universal Imaging Corp., and transferred to Sigma Plot for further processing.

## Results and Discussion

**Binding Data**. A 12-channel microfluidic device fabricated as described above was infused with an SUV solution containing 1.75 mol % DNP-cap PE, 1 mol % fluorescein DHPE, and 97.25 mol % egg PC to form supported lipid bilayers. Solutions of anti-DNP antibodies at different concentrations were infused into each channel and flowed continuously until the bulk concentration remained unchanged as judged by epifluorescence microscopy. Figure 2a shows a total internal reflection image of the surface-bound antibodies across all 12 microchannels. The concentration of antibodies in the first channel was 0.32 $\mu$M and was increased in each subsequent channel until it reached 27.8 $\mu$M in the last one. Background subtraction experiments were needed, since the measured TIRFM signal could arise from specifically bound antibodies, nonspecifically bound antibodies, and antibodies in the near surface bulk solution. This was obtained by monitoring the fluorescence intensity in an identical setup, but without haptens in the bilayer (Figure 2b). The results from both of these experiments are plotted in Figure 2c. As expected, the data from the hapten-containing bilayers showed saturation behavior while the background data were nearly linear. Binding curves in all subsequent experiments reported herein were obtained by subtracting the background data from the signal data.

The 12-channel microfluidic device collected all points on the binding curve simultaneously. Therefore, the apparent
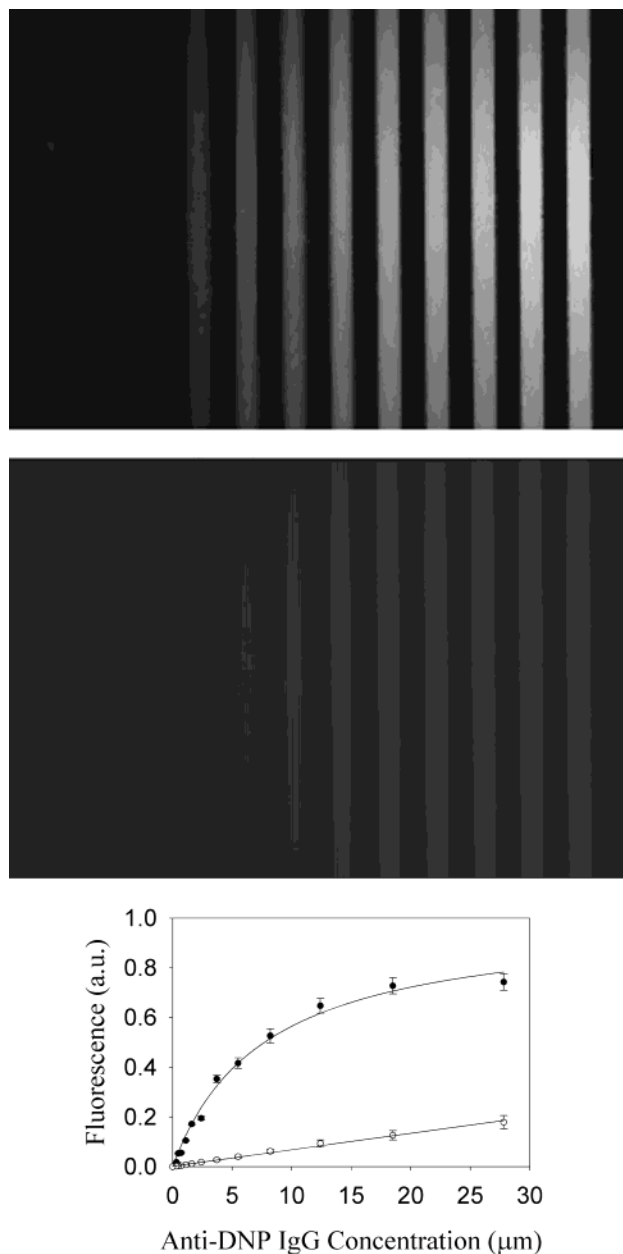


**Figure 2.** (a, top) TIRFM image of various concentrations of fluorescently labeled anti-DNP antibodies binding to egg PC bilayers containing 1.75 mol % DNP-cap PE in a microfluidic array. (b, middle) TIRMF image of anti-DNP antibodies binding to egg PC bilayers without DNP-cap PE lipids. (c, bottom) Fluorescence intensity of surface-bound protein vs bulk protein concentration for 1.75 mol % DNP-cap PE containing bilayers (open circles) and for bilayers without the antigen-linked lipids (solid circles). The solid lines represent least-squares fits to the data. The fluorescence intensities in (a) and (b) were uniform down to the diffraction limit.

binding constant, $K_{Dapp}$, which is equal to the solution concentration of antibodies corresponding to the point at which half-saturation of the surface is achieved,[17,34] could be monitored as a function of time. For the devices employed under the conditions presented here, the fluorescent intensities stabilized after approximately 1 h of incubation and $K_{Dapp}$ remained relatively constant for at least another hour thereafter (Figure 3). This observation suggested that the ligand−receptor interactions approached steady-state conditions, which supports the use

(28) Haugland, R. P. In *Handbook of Fluorescent Probes and Research Products*; Molecular Probes, Inc., 2002; pp 27−29.
(29) Lok B. K., C. Y. L., Robertson C. R. *J. Colloid Interface Sci.* **1983**, *91*, 87−103.
(30) Lok B. K., C. Y. L., Robertson C. R. *J. Colloid Interface Sci.* **1983**, *91*, 104−116.
(31) Axelrod, D.; Burghardt, T. P.; Thompson, N. L. *Annu. Rev. Biophys. Bioeng.* **1984**, *13*, 247−268.
(32) Burmeister, J. S.; Olivier, L. A., Reichert, W. M., Truskey, G. A. *Biomaterials* **1998**, *19*, 307−325.
(33) Hlady, V., Reinecke, D. R., Andrade, J. D. *J. Colloid Interface Sci.* **1986**, *111*, 555−569.

(34) Tamm, L. K.; Bartoldus, I. *Biochemistry* **1988**, *27*, 7453−7458.
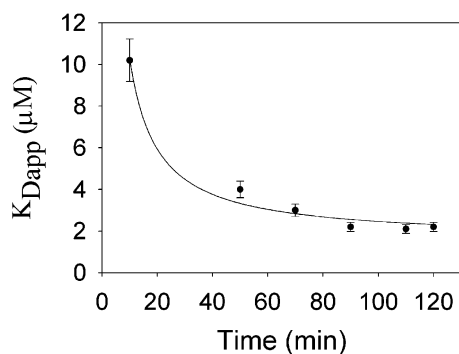
**Figure 3.** Time-dependent changes in the apparent binding constant for antibodies binding to antigen-containing membranes. The solid line is a guide to the eye.
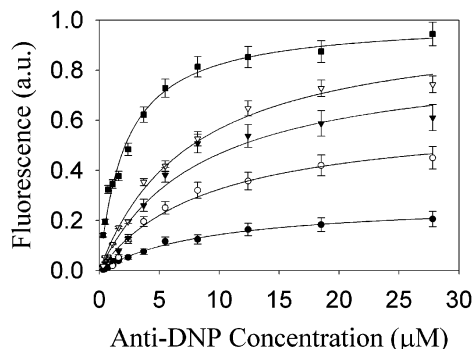


**Figure 4.** Normalized binding curves of antibody binding to lipid bilayers containing 0.1 (solid circles), 0.50 (open circles), 0.75 (solid triangles), 1.75 (open triangles), and 3.75 (solid squares) mol % DNP-cap PE.

**Table 1**

| concn of DNP-cap PE in supported lipid bilayers (mol %) | apparent ligand density (mol/m²) | calcd available ligand density, [L]$_s$ (mol/m²) | % ligand availability | measured $K_{Dapp}$ (M) | fraction of IgG that is bivalently bound |
|---|---|---|---|---|---|
| 0.10 | $2.38 \times 10^{-9}$ | $2.36 \times 10^{-9}$ | 99.0 | $1.8 \times 10^{-5}$ | 0.26 |
| 0.30 | $7.13 \times 10^{-9}$ | $6.90 \times 10^{-9}$ | 96.8 | $1.3 \times 10^{-5}$ | 0.50 |
| 0.50 | $1.19 \times 10^{-8}$ | $1.12 \times 10^{-8}$ | 94.6 | $9.5 \times 10^{-6}$ | 0.62 |
| 0.75 | $1.78 \times 10^{-8}$ | $1.64 \times 10^{-8}$ | 92.0 | $7.6 \times 10^{-6}$ | 0.70 |
| 1.00 | $2.38 \times 10^{-8}$ | $2.13 \times 10^{-8}$ | 89.4 | $5.2 \times 10^{-6}$ | 0.76 |
| 1.75 | $4.16 \times 10^{-8}$ | $3.40 \times 10^{-8}$ | 81.8 | $4.4 \times 10^{-6}$ | 0.83 |
| 2.50 | $5.94 \times 10^{-8}$ | $4.44 \times 10^{-8}$ | 74.8 | $3.7 \times 10^{-6}$ | 0.87 |
| 3.10 | $7.36 \times 10^{-8}$ | $5.14 \times 10^{-8}$ | 69.8 | $2.8 \times 10^{-6}$ | 0.88 |
| 3.75 | $8.90 \times 10^{-8}$ | $5.77 \times 10^{-8}$ | 64.8 | $2.2 \times 10^{-6}$ | 0.89 |
| 4.37 | $1.04 \times 10^{-7}$ | $6.28 \times 10^{-8}$ | 60.4 | $2.0 \times 10^{-6}$ | 0.90 |
| 5.00 | $1.19 \times 10^{-7}$ | $6.74 \times 10^{-8}$ | 56.6 | $1.8 \times 10^{-6}$ | 0.91 |

of equilibrium expressions to analyze the data. All subsequent data reported in this paper were therefore collected after waiting 90 min.

Using the methods described above, binding curves were obtained on supported bilayers as a function of hapten density for 11 concentrations ranging from 0.1 to 5.0 mol % DNP-cap PE in egg PC membranes. In addition to the hapten-conjugated lipid, the membranes contained 1 mol % fluorescein DHPE, and the remainder was egg PC. All data were repeated at least three times, and the results were averaged. Five representative binding curves are shown in Figure 4. A listing of all 11 ligand densities employed is given in the first column of Table 1.

**Monovalent Binding Model.** In the most rudimentary models, ligand−receptor binding data are fit to simple Langmuir isotherms[16,17,34] regardless of the valency of the system under investigation. The parameter extracted from this procedure is the apparent dissociation constant, $K_{Dapp}$, which is equal to the bulk concentration of protein at which half of the maximum
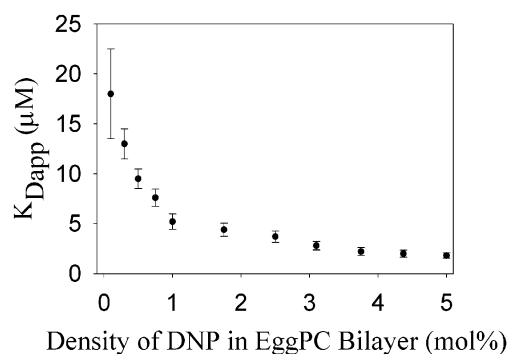


**Figure 5.** $K_{Dapp}$ vs mole percent DNP-cap PE in the lipid bilayers for anti-DNP binding.

coverage is achieved as noted above. The association of a monovalent protein, P, in solution with a binding site, L, on the surface leads to the formation of a membrane-bound complex, PL. The entire process is characterized by a single association constant, $K$:

$$K[P][L]_s = [PL]_s \tag{1}$$

The subscript s after [L] and [PL] denotes surface-associated species. Their concentrations have units of mol/m². The surface hapten moieties are much smaller than the antibodies, so [L]$_s$ represents the surface density of available binding sites, but will be less than the total number of haptens when the bilayer contains a high mole fraction of hapten-conjugated phospho-lipids. The total density of surface sites, [S]$_s$, is

$$[S]_s = [L]_s + [PL]_s \tag{2}$$

The surface-normalized fluorescence can be calculated from the saturation function as previously described:[16]

$$\frac{F([P])}{F([\infty])} = \frac{[PL]_s}{[S]_s} = \frac{K[P]}{1 + K[P]} \tag{3}$$

$F([P])$ is the fluorescent yield when the bulk concentration of fluorescently labeled protein is [P] and $F([\infty])$ refers to the maximum fluorescent intensity when fluorophore-labeled pro-teins completely saturate the membrane surface. In the experi-ments described here, the antibody solution concentration, [P], equaled the applied concentration, $C$, because an antibody solution with a known concentration was continually flowed through the channels until equilibrium was established. The best fit of the experimentally determined fluorescence as a function of [P] yields the values of the surface dissociation constant, $K_{Dapp}$ (which is $1/K$). These values are plotted in Figure 5 as a function of ligand density for the complete set of binding curves described above. The error bars are much larger on the 0.1 mol % data than for the rest of the hapten densities because the signal obtained was only slightly higher than the background that needed to be subtracted. This source of error was a much smaller factor at higher densities. The data show that $K_{Dapp}$ became approximately 1 order of magnitude smaller (tighter) as the ligand density was increased. The decrease continued until about 3.75 mol %, at which point the binding constant appeared to level off.

**Bivalent Binding Model.** Previous efforts have been made to model the surface association in bivalent systems.[16] Beginning

with this notation, two equilibria can be written corresponding to the two sequential binding events:

$$K_{A1} = \frac{[BL]_s}{[B][L]_s} \quad \text{and} \quad K_{A2} = \frac{[BL_2]_s}{[BL]_s[L]_s} \qquad (4)$$

The protein is now represented as B for bivalent. The units of $K_{A1}$ are in $M^{-1}$, while $K_{A2}$ has units of $m^2/mol$ (1/number density). The total surface site density, $[S]_s$, can be expressed as

$$[S]_s = [BL_2]_s + \frac{1}{2}[BL]_s + \frac{1}{2}[L]_s \qquad (5)$$

The surface-normalized fluorescence

$$\frac{F([B])}{F([\infty])} = \frac{[BL]_s + [BL_2]_s}{2[S]_s} \qquad (6)$$

after substitution of eqs 4 and 5 into eq 6 can be written as

$$\frac{F([B])}{F([\infty])} = \frac{\alpha K_A[B]}{1 + K_A[B]} \qquad (7)$$

where

$$K_A = K_{A1} + 2K_{A1}K_{A2}[L]_s \qquad (8)$$

and

$$\alpha = \frac{1 + K_{A2}[L]_s}{1 + 2K_{A2}[L]_s} \qquad (9)$$

In this notation, the bivalent binding model takes on the same general form as the monovalent model and all the experimental binding curves can be fit to a Langmuir isotherm. The term $K_A$ for bivalent binding is now interpreted as an association or affinity parameter for the overall process. $K_A$ is not a constant, as it varies with the ligand density in the membrane, which is being changed in these experiments. It is, however, constant at any fixed ligand density and, hence, does not perturb the shape of the Langmuir isotherms. The parameter $\alpha$, which can vary between 0.5 and 1.0, also depends on ligand density, but like $K_A$ is constant at each fixed density value. The value of $\alpha$ should reach 1.0 when all protein binds monovalently to the surface and fall to 0.5 when binding is entirely bivalent.

Experimental data are typically expressed in terms of dissociation constants, where $K_D = 1/K_A$. Therefore, if the individual dissociation constants are written as $K_{D1}$ and $K_{D2}$, the apparent experimental parameter, $K_{Dapp}$, extracted from the fit to the isotherm can be written as follows:

$$K_{Dapp} = \frac{K_{D1}K_{D2}}{K_{D2} + 2[L]_s} \qquad (10)$$

When $2[L]_s \ll K_{D2}$, $K_{Dapp} \approx K_{D1}$ and eq 10 simplifies to the monovalent model. On the other hand, when $2[L]_s \gg K_{D2}$, $K_{Dapp} \approx K_{D1}K_{D2}/2[L]_s$. Both $K_{D1}$ and $K_{D2}$ can be determined by fitting this equation to the data in Figure 5 provided that $[L]_s$ is known. Apparent values for the number density of ligands can be calculated by noting that the area occupied by an egg PC
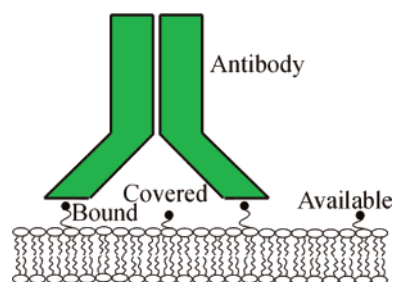


**Figure 6.** Schematic of large IgG antibodies binding to membranes containing small antigens. The ligands are covered, bound, or available.
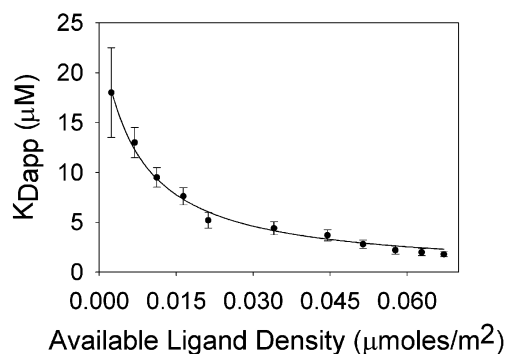


**Figure 7.** Relationship between $K_{Dapp}$ and the available ligand density for anti-DNP antibodies binding to antigen-containing lipid bilayers. The solid line represents a least-squares fit to the data using a hyperbolic function (eq 10).

headgroup is ~70 Å$^2$/molecule[35] and further assuming that DNP-cap PE is roughly the same size. These values are listed in the second column of Table 1. Such values can, however, be perturbed if the binding protein is sufficiently large.[6] In the present case each IgG antibody covers an area of about 60 nm$^2$ on the membrane surface.[34,36] Therefore, some portion of the unbound antigens should be covered by proteins at any given instance (Figure 6). This perturbation to ligand availability becomes greater at higher ligand densities because the average distance between ligand moieties decreases. This effect can be accounted for using an appropriate model for the surface binding of large proteins.[6] The corrected values are listed in column 3 of Table 1, and the explicit calculation used is provided in the Supporting Information for this paper. The results show that almost all the ligands (99.0%) are available at 0.1 mol %, but only 56.8% are available at 5.0 mol %. The percentages of ligands available at all concentrations are listed in column 4 of Table 1.

The corrected values of $[L]_s$ require a recalibration of the *x*-axis for the data in Figure 5. The rescaled data and the curve fit to it from eq 10 are shown in Figure 7. The fitted values of the dissociation constants are

$$K_{D1} = 2.46 \times 10^{-5}\,M$$

$$K_{D2} = 1.37 \times 10^{-8}\,mol/m^2$$

These numbers can be utilized to calculate the corresponding free energy changes for the individual ligand–receptor binding steps. Invoking $\Delta G = -RT \ln K_A$ under the conditions of this

(35) White, S. H.; King, G. I. *Proc. Nat. Acad. Sci. U.S.A.* **1985**, *82*, 6532–6536.
(36) Coleman, P. M.; Deisenhofer, J.; Huber, R. *J. Mol. Biol.* **1976**, 257–282.

experiment ($T = 295$ K) yields

$$\Delta G_1 = -26.0 \pm 0.4 \text{ kJ/mol}$$

$$\Delta G_2 = -44.4 \pm 0.7 \text{ kJ/mol}$$

The decrease in free energy of the second binding event is, therefore, almost a factor of 2 greater than for the first. It should be noted that the activity coefficients are assumed to be unity for obtaining these thermodynamic values.

Once $K_{D2}$ was determined, the $\alpha$ value could be easily calculated for each ligand density using eq 9. The mole fraction that is bivalently bound is equal to $2(1 - \alpha)$. These values are listed in the last column of Table 1. As can be seen, nearly all protein is bivalently bound at the highest hapten density (91%), but at the lowest hapten density only 26% of the IgG molecules are bivalently bound. Moreover, the percent of bivalently bound protein rose steeply at first, with one in two proteins already bivalently bound at 0.3 mol % hapten density and about three out of four proteins bivalently bound at 1.00 mol % hapten density. Above this latter value the percentage of bivalently bound protein rose more slowly toward 100%.

**Comparison between Bulk-Phase and Surface Binding**. The binding of IgG antibodies to hapten-containing membranes is not a directly cooperative process. In other words, no allosteric mechanism is at work and the intrinsic affinity of the second binding event should not be affected by the first. This has been verified by homogeneous-phase binding measurements, where $K_{D2}$ was actually found to be slightly larger (weaker) than $K_{D1}$.[37,38] This was the case because only one binding site is available once a first ligand has bound and there are two choices for unbinding. In other words, entropic considerations lead to $K_{D1} < K_{D2}$ in the homogeneous phase.

For sequential binding at membrane surfaces, there is also an entropic difference between the first and second binding events. In this case the result is the opposite and of much greater magnitude than in the homogeneous phase.[37,38] The difference in entropy at the interface for the two sequential binding events can be calculated by simply assuming that the enthalpy of both events is the same. The free energy of each event can be written as follows:

$$\Delta G_1 = \Delta H_1 - T\Delta S_1 \text{ (first binding event)}$$

$$\Delta G_2 = \Delta H_2 - T\Delta S_2 \text{ (second binding event)}$$

A difference in free energy, $\Delta G_2 - \Delta G_1 = T(\Delta S_1 - \Delta S_2)$, results if the two enthalpy values are assumed to be identical. $\Delta S$ is therefore 62.3 J/(mol·K) higher for the second event than for the first. This difference presumably stems from the fact that the entropic cost of bringing the protein to the surface and properly orienting it is almost entirely borne by the first binding

step. Moreover, the second binding site on the antibody is already at the interface and at least partially aligned and positioned to undergo the subsequent binding step. $\Delta S_2$, therefore, really just contains a lateral diffusion component and the local entropic changes associated with binding (e.g., the displacement of water molecules from the binding pocket upon interaction with the ligand).

The specific contributing factors that lead to the high entropic cost for bringing the antibody to the interface can be considered in two parts. First, as the antibody approaches the lipid surface it must have at least one binding site oriented to face the membrane. Second, a DNP ligand must be properly oriented at the interface for binding to take place. The latter consideration could be particularly important if monovalently bound protein molecules were more readily able to undergo additional binding with haptens partially buried in the lipid bilayer than newly arriving IgG molecules from the bulk solution. It is known that at least under some circumstances that 2,4-dinitrophenyl moieties can be partially buried in the membrane.[39] The entropic factors which lower the initial binding constant are almost certainly lowering the on rate, $k_{on}$, while leaving the off rate, $k_{off}$, unaffected. This argument is bolstered by previous measurements of the off rate for Fab fragments from lipid-linked 2,4-dinitrophenyl moieties in supported membranes which gave values of $k_{off} \approx 1 \text{ s}^{-1}$, a quite standard value.[40]

## Conclusions

High-throughput microfluidic methods offer a convenient route for obtaining data on multivalent ligand−receptor interactions on fluid phospholipid membranes. In the present case, binding data were obtained as a function of hapten density for the binding of anti-dinitrophenyl-KLH IgG antibodies and two dissociation constants were abstracted corresponding to the sequential binding steps. Furthermore, the extent of bivalent versus monovalent binding could be determined at each hapten density. The methods used here should be easily expandable to look at multivalent binding in a variety of systems requiring the presence of two-dimensional fluidity. Indeed, more complex questions which might require obtaining dozens if not hundreds of binding curves can now be addressed rapidly with minimal protein expenditure.

**Supporting Information Available:** Calculations of ligand availability at various hapten densities (PDF). This material is available free of charge via the Internet at http://pubs.acs.org.

JA029469F

(37) Mammen, M.; Gomez, F. A.; Whitesides, G. M. *Anal. Chem.* **1995**, *67*, 3526−3535.
(38) Gargano, J. M.; Ngo, T.; Kim, J. Y.; Acheson, D. W. K.; Lees, W. J. *J. Am. Chem. Soc.* **2001**, *123*, 12909−12910.
(39) Balakrishnan, K.; Mehdi S. Q.; McConnell, H. M. *J. Biol. Chem.* **1982**, *257*, 6434−6439.
(40) Pisarchick, M. L.; Gesty, D.; Thompson, N. L. *Biophys. J.* **1992**, *63*, 215−223.